RSC Advances

PAPER

Cite this: *RSC Adv.*, 2015, **5**, 96483

Co-catalytic mechanism of Au and Ag in silicon etching to fabricate novel nanostructures†

Ruike Li,[a] Meicheng Li,*[ab] Yingfeng Li,[a] Pengfei Fu,[a] Younan Luo,[a] Rui Huang,[a] Dandan Song[a] and Joseph Michel Mbengue[a]

Metal-assisted chemical etching is a very popular method of fabricating silicon nanostructures. For the dissolution and recrystallization of Ag and the inertia of Au, we present a co-catalytic mechanism of silicon etching using non-overlapping Au and Ag nanofilms. Meanwhile, two kinds of novel nanostructures are obtained by changing the relative positions of the two nanofilms. The results show that regardless of whether the Ag or Au nanofilm is the upper layer, the Ag nanofilm will first react to etch the silicon substrate into silicon nanowires (Si NWs). Afterwards, the Au nanofilm will re-etch the Si NWs into thick pillars (Ag upper) or ultrathin porous Si NWs (Au upper). It should be noted that the vertical etching rates of the two layers are not observably different, in contrast to when the Au and Ag nanofilms are used separately, in which the vertical etching rate of the Ag nanofilm is much higher than that of the Au nanofilm. This occurs because the subsequent re-etching process by the Au nanofilm is conducted at multiple surfaces because Au can generate excessive holes during the decomposition of hydrogen peroxide. Furthermore, this study presents a feasible method for the fabrication of individual, thick (~200 nm) silicon pillars and ultrathin (~25 nm) porous Si NWs. These insights are significant for the syntheses of many nanostructures.

Received 16th September 2015
Accepted 30th October 2015

DOI: 10.1039/c5ra19032k

www.rsc.org/advances

Introduction

Silicon nanostructures have attracted a lot of attention in many areas such as microelectronics,[1–3] energy storage,[4] bio-medical devices,[5–7] ultra-sensitive sensors,[8–11] and solar cells.[12–14] Vapor–liquid–solid (VLS) growth has achieved great success in fabricating various silicon nanostructures.[31] However, this technique requires high energy consumption, high vacuum, and other harsh conditions and results in low output and poor reproducibility. To overcome the above drawbacks, the metal-assisted chemical etching (MACE) process has been developed and is gradually becoming one of the most popular methods for fabricating silicon nanostructures. In this technique, the essential reaction occurs between silicon and HF, and a noble metal is employed to accelerate the reaction.[15–17] The noble metal decomposes H_2O_2 and injects holes into silicon substrates by forming a galvanic cell on the metal/silicon interface.

Ag and Au are the most commonly used noble metals. Due to their different physical features, they exhibit quite different etching characteristics.[18,19] In the Ag catalytic etching process, the Ag's hole-generating ability just matches its hole-injecting ability; thus, the silicon is only etched vertically downwards to from sidewall-like, smooth Si NWs.[16] In contrast, in Au catalytic etching, porous Si NWs structures are formed since Au can generate excessive holes.[22] However, to date, there are few reports on the etching process using both Ag and Au. Kim *et al.*[20,21] fabricated Si NWs using an Au and Ag bilayer nanofilm. They demonstrated that the Au nanofilm protects the Ag nanofilm; thus, using such a bilayer can overcome the tapering that occurs when only the Ag nanofilm is used. In their work, the bilayer nanofilm was synthesized by a template method; therefore, the two layers were completely overlapping so that only the underlying Ag nanofilm served in a catalytic role. If the Au and Ag layers are not overlapping, the etching process should become much more complex and follow a co-catalytic mechanism.

In this study, we first compared the vertical etching rates of individual Au and Ag nanofilms. The vertical etching rate of the individual Ag nanofilm was found to be much higher than that of the Au nanofilm. The co-catalytic mechanism of the Au and Ag bilayer nanofilm was then investigated by analyzing the etching features. We found that during the co-catalytic etching processes of non-overlapping bilayer nanofilms, the Ag nanofilm first etches the silicon substrate into sidewall-like smooth Si NWs. Subsequently, the Au nanofilm re-etches them. When the Ag nanofilm is the upper layer, thick silicon pillars are

[a]*State Key Laboratory of Alternate Electrical Power System with Renewable Energy Sources, North China Electric Power University, Beijing, 102206, China. E-mail: mcli@ncepu.edu.cn*

[b]*Chongqing Materials Research Institute, Chongqing, 400707, China*

† Electronic supplementary information (ESI) available: SEM image of no existence of the Ag nanofilm, SEM image of existence of the Au nanofilm. See DOI: 10.1039/c5ra19032k

obtained; in contrast, when the Au nanofilm is the upper one, ultrathin porous Si NWs are obtained. This study enriches our understanding of the fundamental principles in MACE and guides the fabrication of new types of silicon nanostructures.

Experimental

Materials

Silicon wafers (N (100), resistivity of 2–4 Ω cm) were purchased from China Electronics Technology Group Corporation No. 46 Research Institute, China. H_2O_2 and HF were purchased from Aladdin Industrial (Shanghai) Co. Ltd, Shanghai.

Substrate preparation

The silicon substrates were prepared in three steps. First, the silicon wafer was cut into 10 mm × 10 mm pieces. The silicon pieces were then cleaned by acetone (5 min), anhydrous ethanol (5 min), and DI water (10 min) under ultrasonic conditions at room temperature. Subsequently, they were dipped into a solution of diluted HF (5 mol L^{-1}) for 5 min to remove native oxides. Finally, the cleaned pieces were dried by pure nitrogen gas flow and moved to a vacuum drying chamber (60 °C) as soon as possible in order to avoid contamination.

Nanofilm deposition

Noble metal nanofilms were deposited using a magnetron sputtering apparatus (Quorum Q150-TS) after the silicon substrates had been treated by UV for 15 min.[23] For the etching process using either the Ag or Au nanofilm, the thickness was 5 nm. For the etching process using the Au and Ag bilayer nanofilm (when Ag covers Au, the biofilm is described as Au/Ag; when Au covers Ag, it is referred to as Ag/Au), the thicknesses of the Ag and Au sub-layers are 4 and 2 nm, respectively.

Catalytic etching process

After deposition, the silicon substrates were dipped into the ternary etchant (HF 5 mol L^{-1}, H_2O_2 0.5 mol L^{-1}) for 5 min at 25 °C (maintained by water bath). Finally, the silicon substrates were quickly taken out and rinsed with plenty of DI water to remove the residual etchant.

During the etching procedure, a galvanic cell is formed on the metal/silicon interface, which can greatly accelerate the etching. The reaction equations[24] are:

$$\text{Cathode: } H_2O_2 + 2H^+ \rightarrow 2H_2O + 2h^+ \quad (1)$$

$$\text{Anode: } Si + 4HF_2^- \rightarrow SiF_6^{2-} + H_2\uparrow + 2e^- \quad (2)$$

In this etching process, the holes generated during cathodic reduction are attracted to the metal nanofilm by image force, the electrostatic force on a charge in the neighborhood of a conductor, and injected into the silicon substrate.[18] This hole injection leads to the oxidation of the silicon atoms into silica, which can be rapidly dissolved by the HF. The hole injection mainly occurs at the metal/silicon interface, making the vertical etching rate at this location much higher than in other places.

Characterization

In our study, the morphologies of the nanostructures were characterized by scanning electron microscopy (SEM; FEI Quanta 200F). The porous structure of a single silicon nanowire was characterized by transmission electron microscopy (TEM; ZEISSLIBRA 200 FE).

Results and discussion

To investigate the co-catalytic etching mechanism of the Au and Ag bilayer nanofilm, the etching characteristics using the individual Ag or Au nanofilm were first studied. Then, catalytic etching using bilayer nanofilms with the Ag or Au nanofilm on the upper layer was carried out, and the results were carefully analyzed.

Etching features using Ag and Au separately

The etching characteristics of the Ag and Au nanofilms are of great help in understanding the co-catalytic mechanism of them together. Fig. 1a and b show the Si NW morphologies etched for 5 min by the Ag and Au nanofilms, respectively. All other experimental conditions were the same (HF 5 mol L^{-1}, H_2O_2 0.5 mol L^{-1}, 25 °C). The vertical etching rates can be analyzed by comparing the lengths of the Si NWs.

We can see that the lengths of the Si NWs using the Ag nanofilm as catalyst are about 2 μm, while the lengths of Si NWs obtained using the Au nanofilm are only about 500 nm. This indicates that the Ag nanofilm has a much better catalytic ability than the Au nanofilm. Based on repeated experiments, we have calculated the average vertical etching rates obtained using individual Ag and Au nanofilms as the catalysts; as shown in Table 1, their values are 6.91 and 1.78 nm s^{-1}, respectively.

The superior catalytic ability of the Ag nanofilm can be mainly attributed to fact that the Ag nanofilm can be oxidatively dissolved in H_2O_2 and then recrystallized into nanoparticles. Small particles can contact the silicon substrate more

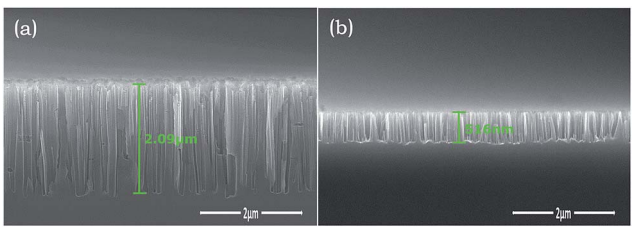

Fig. 1 SEM images of the cross-sectional morphologies etched by individual (a) Ag and (b) Au nanofilms.

Table 1 Vertical etching rates obtained using individual Ag and Au nanofilms as catalysts

Catalyst	1	2	3	4	5	6	AVG	RMSE
Ag (nm s^{-1})	7.0	6.8	7.2	7.3	6.4	6.8	6.9	0.3
Au (nm s^{-1})	1.8	2.0	1.9	1.6	1.7	1.7	1.8	0.1

effectively; therefore, the catalytic activity of the Ag nanofilm can be greatly improved. However, Au is inert with respect to oxidative dissolution and thus cannot be dispersed into nanoparticles.[20] The inertia of Au can be directly verified by the fact that after the etching process, the Au nanofilm can still be observed, as shown in the ESI.†

Catalytic etching by the Au/Ag bilayer nanofilm

For etching using the bilayer catalyst, the case in which the Ag nanofilm is the upper layer was first investigated. To understand the etching process, a series of experiments with etching times ranging from 30 s to 5 min was carried out. The etchant (HF and H_2O_2) concentrations were the same as were used in the above section (HF, 5 mol L^{-1}; H_2O_2, 0.5 mol L^{-1}). Fig. 2 shows the SEM images of the cross-sectional morphologies etched for 30 s, 1 min, 3 min, and 5 min.

After 30 s, short Si NWs with heights of about 200 nm were obtained, as shown in Fig. 2a. Therefore, the vertical etching rate was $v \approx 200$ nm/30 s ≈ 6.7 nm s^{-1}. It should be noted that this value is very close to that obtained using the Ag nanofilm alone (6.9 nm s^{-1}). This indicates that in this time period, the etching process is mainly dominated by the Ag nanofilm. Because the Ag nanofilm can easily be dissolved and recrystallized into nanoparticles, a reasonable etching process for this stage is that depicted in Fig. 3a–c. In this stage, the Ag nanofilm first transforms into nanoparticles, which penetrate into the interspaces of the Au nanofilm and etch the silicon substrate into Si NWs. Because the vertical etching rate of the Ag nanofilm is much higher that of the Au nanofilm, as mentioned above, the Au nanofilm should be on top of the Si NWs.

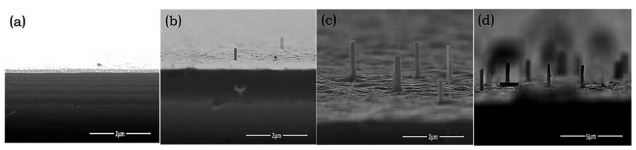

Fig. 2 SEM images of the cross-sectional morphologies etched by the Au/Ag bilayer nanofilm for (a) 30 s, (b) 1 min, (c) 3 min, and (d) 5 min.

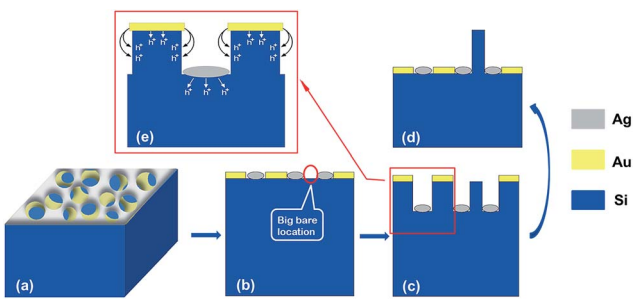

Fig. 3 Illustration of the etching process using the Au/Ag bilayer nanofilm. (a) Au/Ag bilayer nanofilm. (b) The interspaces of the Au nanofilm are filled up by crystallized Ag nanoparticles. (c) Formation of sidewall-like Si NWs. (d) Formation of a sporadic Si pillar. (e) Hole-injection process from the Au nanofilm to the Si NWs.

Fig. 2b shows that after 1 min, the Si NWs had disappeared, except for some scattered thick pillars with heights of about 400 nm. The calculated vertical etching rate was 400 nm/60 s ≈ 6.7 nm s^{-1}, which is still close to the vertical etching rate obtained using the Ag nanofilm alone. This means that the vertical etching rate was determined by Ag as before. Because the vertical etching rate of the individual Au nanofilm is much lower than that of the Ag nanofilm, it can be logically concluded that a sidestep-like structure will result. However, in practice, no sidestep-like structure appeared. This can be rationally explained as follows. Au can generate excessive holes during H_2O_2 decomposition; thus, in the re-etching process conducted by the Au nanofilm, hole injection not only occurs at the Au/Si interface, but also at the nearby sidewall nearby. Therefore, the etching actually takes place at multiple surfaces simultaneously, as shown in Fig. 3d and e. The multi-surface etching greatly enhances the vertical etching rate of the Au nanofilm, which even reaches the vertical etching rate of the Ag nanoparticles. As a consequence, almost the entire silicon surface is etched down by the Au nanofilm with the exception of the big bare locations not covered by the Ag or Au nanofilm. This also provides a logical explanation for the disappearance of the Si NWs and the appearance of the sparse pillars.

With the increase in etching time from 3 to 5 min, the height of the silicon pillars increased gradually, as shown in Fig. 2c and d. The calculated vertical etching rates are about 6.7 and 7.9 nm s^{-1}, respectively, which are also consistent with the above rate obtained by Ag etching.

The thick Si pillars we fabricated can be used as substrates for the growth of carbon nanotubes[25,32–34] and Cu nanofilms.[26] In addition, they may also have great potential in broadband heterojunction photodetector manufacturing engineering.[27,28]

Catalytic etching by the Ag/Au bilayer nanofilm

We also carried out experiments in which the silicon substrate was etched by the Ag/Au nanofilm for 5 min. Because the Ag nanofilm was beneath the Au nanofilm, the etching area of the Ag nanofilm no longer depended on the apertures of the Au nanofilm in the initial stage. The actual etching process should be a kind of double-screen process by the Ag and Au nanofilm, as shown in Fig. 4. In this process, the Ag nanofilm first etches the silicon into vertical sidewall-like smooth Si NWs. Soon afterwards, the Au nanofilm re-etches the Si NWs into ultrathin porous Si NWs.

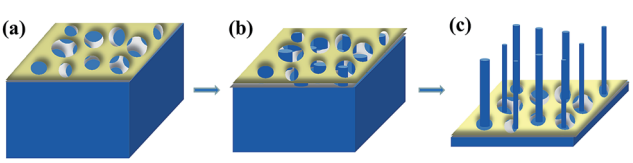

Fig. 4 The schematic diagram of the Ag/Au nanofilm catalytic etching process. (a) The Ag/Au bilayer nanofilm. (b) The crystallized Ag nanoparticles etch the silicon substrate into sidewall-like Si NWs. (c) The Au nanofilm re-etches the Si NWs into ultrathin porous Si NWs.

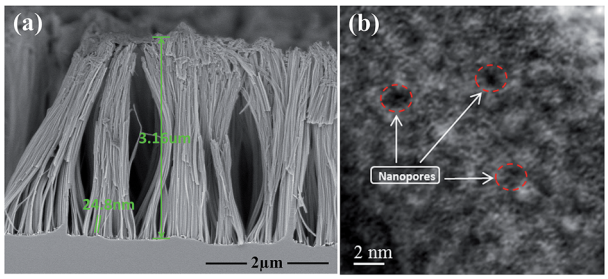

Fig. 5 (a) SEM image of the cross-sectional morphology of ultrathin porous Si NWs. (b) HRTEM image of the surface of a single ultrathin porous Si NW.

The etching morphology is shown in Fig. 5a. Homogeneous ultrathin Si NWs were obtained. Their average diameter was about 25 nm, which can be ascribed to the double-screen effect. The much larger density of the Si NWs compared to those etched by the Au/Ag nanofilm clearly indicates a greatly different etching mechanism. The HRTEM image of the surface of an individual nanowire shown in Fig. 5b indicates that the nanowire is covered by dense and homogeneous nanoscale pores. These pores, marked by red dotted circles, have diameters of about 2 nm. The formation of these pores was due to the catalytic etching effect of the Au nanofilm. A metal's catalytic activity is related to its ability to decompose H_2O_2 and seize electrons from silicon. In the etching stage by Ag, the hole-generating ability of the cathodic reduction reaction matches the hole-injecting ability. Therefore, the silicon substrate will only be etched vertically, leading to the formation of sidewall-like Si NWs. In the Au etching stage, because Au's hole-generating ability is much stronger than its hole-injecting ability, excessive holes will exist. These excessive holes can escape the image force of the Au nanofilm and diffuse to the sidewall of the Si NWs. That is, the hole-injection not only occurs in the Au/Si interface, but also on the sidewalls of the Si NWs. The hole-injection on the sidewalls leads to the formation of the pores.

The ultrathin porous Si NWs may have great potential in a wide range of applications due to their ultrathin and porous properties. For example, both of these features can greatly improve the abilities of lithium batteries to store electric charges.[29,30]

Conclusions

In summary, the co-catalytic etching mechanism is due to the synergetic action of Ag- and Au-assisted etching. The quick etching feature of Ag can effectively complement the inertia of Au and bring about the first etching of the silicon into nanowires catalyzed by the Ag film. Subsequently, the excellent hole-generating ability of Au will bring in the 3D etching of Si NWs, which results in a high vertical etching rate and the formation of extraordinary nanostructures. In detail, the Ag nanofilm first takes part in the etching process, and the Au nanofilm then conducts the subsequent etching procedure. In the initial step, the Ag nanofilm etches the silicon substrate downwards to form sidewall-like Si NWs. In the latter step, when the Ag nanofilm is on the upper layer, thick silicon pillars are obtained; when the Ag nanofilm is in the lower layer, ultrathin porous Si NWs are obtained. Notably, the vertical etching rates of the two layers do not show observable differences. In contrast, when the layers are used separately, the vertical etching rate of the Ag nanofilm is much higher than that of the Au nanofilm. We attribute this synchronism to the fact that Au can generate excessive holes during H_2O_2 decomposition; hole injection not only occurs at the Au/Si interface, but also at the sidewall nearby in the re-etching process. That is to say, the Au nanofilm simultaneously etches multiple surfaces. The mechanisms we proposed could provide guidance for the fabrication of a wide range of nanostructures. This study also provides feasible ways to fabricate single silicon pillars and ultrathin porous Si NWs.

Acknowledgements

This work is supported partially by the National High-tech R&D Program of China (863 Program, No. 2015AA034601), National Natural Science Foundation of China (Grant no. 91333122, 51402106, 51372082, 51172069, 61204064 and 51202067), Ph.D Programs Foundation of Ministry of Education of China (Grant no. 20120036120006, 20130036110012), Par-Eu Scholars Program, and the Fundamental Research Funds for the Central Universities.

Notes and references

1 G. D. Yuan, Y. B. Zhou, C. S. Guo, W. J. Zhang, Y. B. Tang, Y. Q. Li, Z. H. Chen, Z. B. He, X. J. Zhang, P. F. Wang, I. Bello, R. Q. Zhang, C. S. Lee and S. T. Lee, *ACS Nano*, 2010, **4**, 3045–3052.
2 Y. Cui and C. M. Lieber, *Science*, 2001, **291**, 851–853.
3 L. J. Chen, *J. Mater. Chem.*, 2007, **17**, 4639–4643.
4 K. Peng, J. Jie, W. Zhang and S. T. Lee, *Appl. Phys. Lett.*, 2008, **93**, 033105.
5 B. H. Zhang, H. S. Wang, L. H. Lu, K. L. Ai, G. Zhang and X. L. Cheng, *Adv. Funct. Mater.*, 2008, **18**, 2348–2355.
6 S. Wang, H. Wang, J. Jiao, K. Chen, G. E. Owens, K. Kamei, J. Sun, D. J. Sherman, C. P. Behrenbruch, H. Wu and H. Tseng, *Angew. Chem., Int. Ed.*, 2009, **48**, 8970–8973.
7 M. L. Zhang, C. Q. Yi, X. Fan, K. Q. Peng, N. B. Wong, M. S. Yang, R. Q. Zhang and S. T. Lee, *Appl. Phys. Lett.*, 2008, **92**, 043116.
8 Y. Cui, Q. Wei, H. Park and C. M. Lieber, *Science*, 2001, **293**, 1289–1292.
9 M. W. Shao, H. Yao, M. L. Zhang, N. B. Wong, Y. Y. Shan and S. T. Lee, *Appl. Phys. Lett.*, 2005, **87**, 183106.
10 G. F. Zheng, F. Patolsky, Y. Cui, W. U. Wang and C. M. Lieber, *Nat. Biotechnol.*, 2005, **23**, 1294–1301.
11 F. Patolsky, B. P. Timko, G. H. Yu, Y. Fang, A. B. Greytak, G. F. Zheng and C. M. Lieber, *Science*, 2006, **313**, 1100–1104.
12 M. D. Kelzenberg, S. W. Boettcher, J. A. Petykiewicz, D. B. Turner-Evans, M. C. Putnam, E. L. Warren, J. M. Spurgeon, R. M. Briggs, N. S. Lewis and H. A. Atwater, *Nat. Mater.*, 2010, **9**, 239–244.

13 F. Bai, M. C. Li, R. Huang, Y. F. Li, M. Trevor and K. P. Musselman, *RSC Adv.*, 2014, **4**, 1794–1798.
14 Y. F. Li, M. C. Li, R. K. Li, P. F. Fu, L. H. Chu and D. D. Song, *Appl. Phys. Lett.*, 2015, **106**, 091908.
15 F. Bai, M. C. Li, R. Huang, D. D. Song, B. Jiang and Y. F. Li, *Nanoscale. Res. Lett.*, 2012, **7**, 557.
16 F. Bai, M. C. Li, D. D. Song, H. Yu, B. Jiang and Y. F. Li, *J. Solid State Chem.*, 2012, **196**, 596–600.
17 F. Bai, M. C. Li, P. F. Fu, R. K. Li, T. S. Gu, R. Huang, Z. Chen, B. Jiang and Y. F. Li, *APL Mater.*, 2015, **3**, 056101.
18 M. K. Dawood, S. Tripathy, S. B. Dolmanan, T. H. Ng, H. Tan and J. Lam, *J. Appl. Phys.*, 2012, **112**, 073509.
19 M. A. Lachiheb, N. Nafie, M. B. Rabha and M. Bouaïcha, *Phys. Status Solidi C*, 2014, **11**, 337–343.
20 J. Kim, H. Han, Y. H. Kim, S. H. Choi, J. C. Kim and W. Lee, *ACS Nano*, 2011, **5**, 3222–3229.
21 J. Kim, Y. H. Kim, S. H. Choi and W. Lee, *ACS Nano*, 2011, **5**, 5242–5248.
22 C. L. Lee, K. Tsujino, Y. Kanda, S. Ikeda and M. Matsumura, *J. Mater. Chem.*, 2008, **18**, 1015–1020.
23 F. Bai, M. C. Li, R. Huang, Y. Yu, T. S. Gu, Z. Chen, H. Y. Fan and B. Jiang, *J. Nanopart. Res.*, 2013, **15**, 1915–1921.
24 D. Wang, R. Ji, S. Du, A. Albrecht and P. Schaaf, *Nanoscale Res. Lett.*, 2013, **8**, 42.
25 H. S. Uh and S. Park, *Diamond Relat. Mater.*, 2015, **54**, 74–78.
26 X. H. Yang, Z. G. Chen, W. F. Jiang, F. G. Zeng and X. J. Li, *Mater. Sci. Semicond. Process.*, 2013, **16**, 747–751.
27 W. T. Lai, P. H. Liao, A. P. Homyk and A. Scherer, *IEEE Photonics Technol. Lett.*, 2013, **25**, 1520–1523.
28 M. Melvin, D. Kumar, J. H. Yun and J. Kim, *Infrared Phys. Technol.*, 2015, **69**, 174–178.
29 H. C. Tao, L. Z. Fan and X. H. Qu, *Electrochim. Acta*, 2012, **71**, 194–200.
30 X. F. Chen, Y. Huang, J. J. Chen, X. Zhang, C. Li and H. J. Huang, *Ceram. Int.*, 2015, **41**, 8533–8540.
31 S. H. Lee, T. Lee, K. Moon and J. M. Myoung, *ACS Appl. Mater. Interfaces*, 2013, **5**, 11777–11782.
32 P. Zhou, X. Yang, L. He, Z. M. Hao, W. Luo, B. Xiong, X. Xu, C. J. Niu, M. Y. Yan and L. Q. Mai, *Appl. Phys. Lett.*, 2015, **106**, 111908.
33 Z. L. An, L. He, M. Toda, G. Yamamoto, T. Hashida and T. Ono, *Microsyst. Technol.*, 2014, **20**, 201–208.
34 L. He, M. Toda, Y. Kawai, H. Miyashita, M. Omori, T. Hashida, R. Berger and T. Ono, *J. Nanotechnol.*, 2015, **26**, 195601.